Ultra-Low Power Low-Noise Amplifier Design for IoT-Based Tire Pressure Monitoring System

Raya O. Jaradat[1*] iD , Hani H. Ahmad[2] iD , Ala Alzidaneen[3] iD ,

Mohammad A. Ben Tarief[4] iD

[1, 3] Electrical Engineering Department, Al-Karak College, Al-Balqa Applied University, Al-Karak, Jordan.
E-mail: raya.jaradat@bau.edu.jo
[2] Electrical Engineering Department, College of Engineering, Princess Sumaya University for Technology, Amman, Jordan.
[4] Engineering Department, Al-Karak College, Al-Balqa Applied University, Al-Karak, Jordan.

Abstract— The Internet of Things (IoT) nodes and applications have been expanding rapidly; thereby driving the increasing need for ultra-low power RF front-end circuit design, particularly for battery-powered applications. This work presents a highly efficient ultra-low power low-noise amplifier (LNA) circuit designed particularly for IoT tire pressure monitoring system (TPMS) applications. With an inductive degenerated cascode topology, the proposed LNA achieves low noise figure, high gain, and highly efficient power consumption. As determined through comprehensive simulations conducted using the TSMC CMOS 0.18 μm technology, the LNA's superior performance exhibits a noise figure as low as 2.7 dB, high gain of 20.52 dB, and low power consumption of 0.1 mW in the most efficient state. Thus, LNA can possibly enhance TPMS sensitivity and reliability substantially, representing an advancement in IoT technology adaptability across varying applications.

Keywords— Tire pressure monitoring system; IoT; Low-noise amplifier; CMOS; Wireless communication.

1. INTRODUCTION

With the advent of (IoT), a transformative paradigm is introduced, where an expansive array interconnected devices enables seamless sharing of data and communication across various sectors, thus remodeling conventional practices and promoting innovation. IoT devices are majorly used in smart homes to improve energy efficiency and security. In healthcare, IoT of medical things (IoMT) aid in remote monitoring of patients and wearable devices allow the collection of health data in real-time. Industrial IoT (IIoT) has improved automation and predictive maintenance in industries, which has augmented the operational efficiency. Moreover, with the integration of IoT technologies into smart cities, agriculture, and retail, traffic management, precision farming, and supply chain optimization, respectively, have advanced.

Reliable communication protocols (e.g., AMQP, MQTT, HTTP/HTTPS, CoAP, and Bluetooth/Bluetooth Low Energy) determine the effectiveness of IoT applications. While serving as the communicative pillar, these protocols meet the different requirements of IoT scenarios. This paper explores the design considerations of low-noise amplifiers (LNAs) for IoT applications, along with elucidation of the challenges encountered with adapting these

amplification components to meet the unique characteristics and demands of the aforementioned domains.

Tire pressure monitoring systems (TPMS) are essential for enhancing the safety and performance of modern vehicles. Sophisticated electronics, especially radiofrequency (RF) components, are a critical part of TPMS design and are integrated into the systems to ensure precise and consistent tire pressure measurements. Of them, LNAs are crucial for elevating the sensitivity and performance of TPMS sensors, because they amplify weak signals emitted by the sensors with minimal additional noise [1]. With an increase in the demand for TPMS, research interest in developing more sensitive, efficient, and reliable LNAs for these applications is elevating [1].

LNAs, which are electronic circuits essential for RF and microwave systems, amplify weak signals but introduce minimal additional noise. In TPMS, they intensify faint signals from tire pressure sensors, thus enabling to detect and measure tire pressure levels accurately. LNA topology substantially affects system gain, noise performance, bandwidth, and power efficiency; therefore, choosing the correct topology is important. However, several difficulties are encountered while designing and implementing LNAs for IoT applications [2]. One such challenge is to design ultra-low-power LNAs so that battery life can be extended, while another challenge is to achieve the wide bandwidth required by LNAs to support diverse communication protocols employed in IoT applications.

In this paper, the advanced LNA design for TPMS, an IoT application, is discussed. We here elaborate and compare the performance of various LNA types for power consumption, bandwidth, and noise characteristics. Additionally, IoT applications utilizing LNAs are surveyed. The study provides beneficial insights to researchers and engineers for developing innovative LNA designs suited for IoT applications. In subsequent sections, we comprehensively review LNA designs currently used in TPMS and compared their performance metrics, including noise figure, power consumption, and linearity. By meticulously surveying LNA-employing TPMS applications, we elucidate the unique needs of each application scenario. This study specifically examines the basics to be considered while choosing LNA topologies for TPMS applications, such as Common Collector (CC), Common Base (CB), Common Emitter (CE), Differential, and Cascode configurations [2].

This research aims to comprehend the variations in LNA configurations, thereby enhancing TPMS designs, offering accurate tire pressure measurements, and elevating vehicle safety standards. To achieve these objectives, each topology was carefully assessed for its strengths and drawbacks in relation to TPMS performance criteria. This meticulous assessment offered major insights about automotive electronics and RF engineering and a valuable guidance for engineers and researchers committed to improving the efficiency and accuracy of TPMS devices. This study thus seeks to increase vehicle safety and performance, broadening the field of IoT applications.

2.   REVIEW OF LNA TOPOLOGIES

LNAs with varying topologies that can meet specific demands and performance requirements have been fabricated. The CE topology, which has high voltage gain and moderate input/output impedance, is applied in RF amplification for its moderate noise figure and satisfactory gain characteristics. Owing to its low input impedance and high current gain, the CB configuration is fit for high-frequency applications, which need impedance matching

[2]. The CC topology (or emitter follower) offers high input impedance and unity voltage gain and so is best suited for buffering and impedance transformation [3]. Offering a well-balanced blend of high gain, wide bandwidth, and good linearity, the Cascode topology, which integrates common emitter and common base stages, is expedient in RF and microwave systems [4]. The Differential configuration is predominantly employed in communication systems requiring balanced signaling and noise suppression. This configuration is known for its excellent common-mode rejection [3].

Using inductive elements, LNAs with inductive feedback attain high noise performance and gain, especially at higher frequencies. Characterized by high current and voltage gain, the Darlington topology is suitable for applications in which power must be substantially amplified. Selecting an appropriate LNA topology relies on certain application requirements, such as gain, noise figure, bandwidth, and impedance matching, ensuring optimal performance across various RF and microwave systems [5]. Fig.1 presents the key topologies of Low Noise Amplifiers (LNAs), which are essential components in communication systems for signal amplification with minimal noise addition.
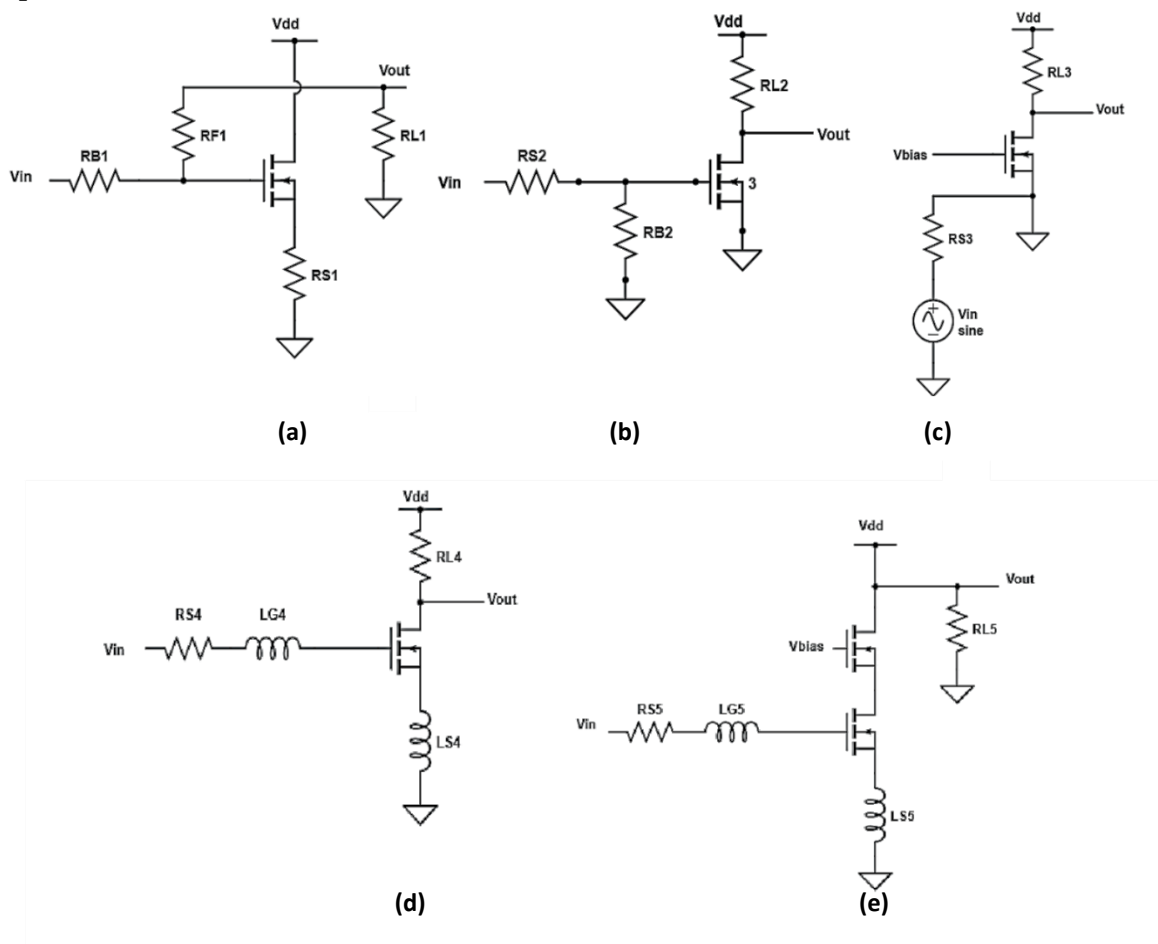
Fig. 1. Key LNA topologies: a) common source (CS) LNA with shunt-series feedback; b) CS LNA with resistive termination; c) common gate (CG); d) inductive degeneration common source LNA (IDCS); e) inductive source degeneration LNA in cascode configuration.

The TREAD Act [6] spurred the extensive adoption of TPMS in the United States, following the Ford-Firestone tire failure incident [7]. In addition to preventing tire failures, alerting drivers to low tire pressure enhances safety on roads and fuel economy, as optimal tire inflation boosts traction, reduces braking distances, and minimizes rolling resistance.

TPMS continuously tracks the air pressure inside the tires of cars, trucks, and multipurpose vehicles, notifying drivers about a significantly underinflated tire. Although both direct and indirect methods are used for measuring air pressure, only direct methods meet the TREAD Act's measurement sensitivity standards and are currently in use.

Due to the challenges of establishing a wired connection between a rotating tire and the electronic control unit of the vehicle, the sensor module uses an RF transmitter to relay data. The receiving tire pressure control unit processes these data and communicates with the vehicle's main computer via the Controller-area Network, often triggering dashboard warnings. Indirect measurement methods, in contrast, infer tire pressure changes from differences in rotational speed, detectable through anti-lock braking system sensors. A tire with lower pressure must rotate faster to cover equal distance as a higher-pressure tire. However, this method has limitations, including reduced accuracy, the need for driver calibration, and an inability to detect simultaneous tire pressure drops (e.g., due to temperature changes).

3.   TPMS ARCHITECTURE

TPM sensors fitted into the back of each tire's valve stem, a TPM electric control unit (ECU), a receiving unit (either integrated with the ECU or stand-alone), a dashboard TPM warning light, and one or four antennas connected to the receiving unit are typical components of a direct TPMS.

Starting in 2007, all tires and vehicles have to be TPMS enabled so every new tire you put on your car contains a module that senses various aspects of your tire and wirelessly communicates the information to the car's brain. The details vary between systems and automotive manufacturers, but the basic block diagram is shown in Fig. 2. TPM sensors broadcast pressure and temperature values together with their identifiers on a regular basis. Before transmitting messages to the TPM warning light.
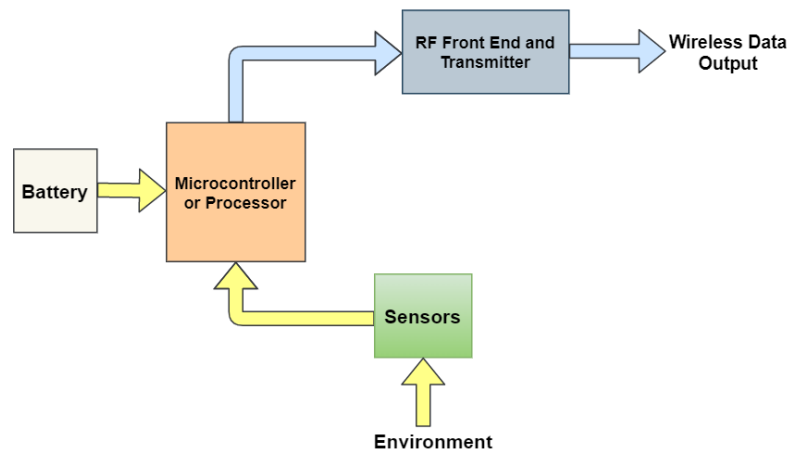

Fig. 2. Basic block of TPMS diagram.

The TPM ECU/receiver receives the packets and conducts the following activities. First, because it can receive packets from sensors on other automobiles, it filters them out. Second, it compensates for temperature by normalizing pressure data and evaluating tire pressure variations. The precise architecture of the system varies depending on the provider, especially in terms of antenna arrangement and communication protocols. In high-end automobile models, a four-antenna setup is common, with an antenna fitted in each wheel housing under

the wheel arch shell and connected to a receiving unit by high-frequency antenna wires, as shown in Fig. 3. Because the antennas are positioned near to the TPM sensors, the four-antenna system extends sensor battery life by lowering the needed sensor transmission power. However, in order to lower vehicle costs, the majority of car manufacturers employ a single antenna, which is commonly located on the rear window [8-9].
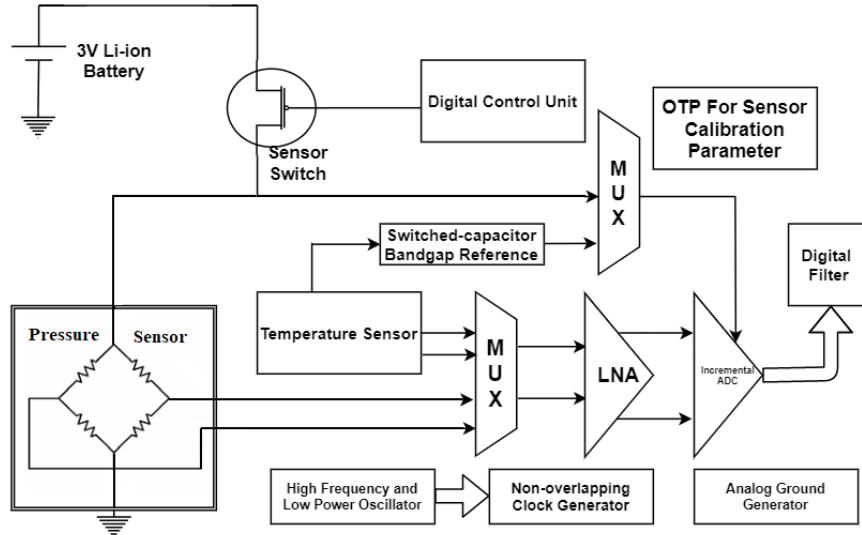

Fig. 3. Hardware design block diagram of TPMS transmitter.

4.   COMMUNICATION PROTOCOLS

The protocols for communication between sensors and TPM ECUs are special to each company. But TPMS often use 315 MHz or 433 MHz frequency (UHF) with ASK (Amplitude Shift Keying) or FSK (Frequency Shift Keying) modulation. Each tire sensor has a unique ID. Before the TPMS ECU can read data from sensors, their IDs and the position of the wheel where it is must be input manually in most cars or automatically in some expensive ones. This is usually done when installing tires. After that, the sensor ID is very important because it helps ECU know where data come from and ignore signals from other.

Fig. 4 shows the block diagram of receiver [10]. There are two main processing paths based on the type of modulation. One path is for sensors using ASK modulation, and the other one is for sensors using FSK modulation. The receiver can get signals from seven types of TPMS sensors, and it has a range of about 100 m with directional antenna. When signal is received correctly, the receiver ID, sensor ID, sensor type, and time are saved into database for later processing.
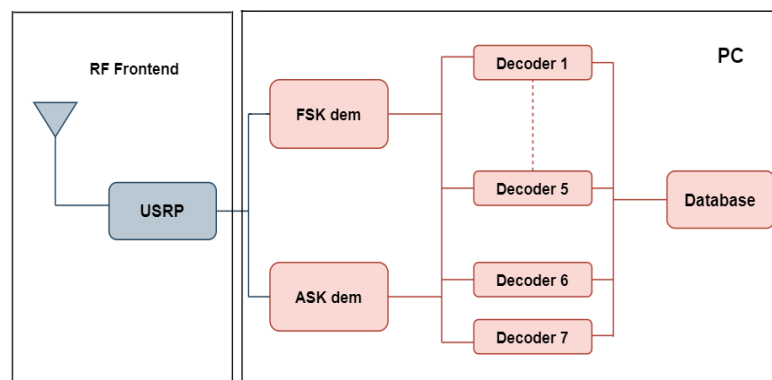

Fig. 4. Structure of the prototype TPMS receiver.

5. THE PROPOSED LNA SCHEMATIC AND DESIGN STEPS

Designing an LNA for IoT-based TPMS entails balancing ultra-low power consumption, high gain, and low noise figure. The proposed LNA, based on the Inductive Degenerated Cascode (IDCS) topology, effectively balances these critical requirements. The design for this LNA mainly focused on reducing power consumption, lowering the noise figure, and maximizing gain. Reduction of power consumption prolongs the battery life of TPMS devices and ensures long-term use of these devices in energy-restricted settings. System's sensitivity is boosted with a low noise figure, which aids in detecting weak signals precisely even under challenging conditions. Moreover, maximum gain is essential to deliver an adequately strong, amplified signal for further processing without notable degradation, thereby preserving the system's performance and reliability.

During the design process, initially, an appropriate amplifier topology is chosen according to the application's needs, focusing on factors such as gain, linearity, power consumption, and noise figure. Because the LNA proposed here uses the IDCS topology with outstanding attributes and was therefore compatible with IoT applications. Strict power constraints are usually experienced during the operation of IoT devices while they require reliable communication protocols. The IDCS topology excels as it attains a high gain, a low noise figure, and strong linearity simultaneously; these are traits essential for managing weak signals in challenging environments of IoT applications [11]. The robust design of LNA allows for the efficient use of power, which makes it best for battery-powered IoT devices, and the delivery of consistent performance across varying temperature conditions and manufacturing processes. Furthermore, the topology's simplified structure and compatibility with CMOS technology align well with the compact, integrated design often used in IoT devices, which renders it a great choice for boosting sensitivity and extending wireless communication range in IoT applications [12-16].

The second step involves identifying ideal device sizes and biasing voltages to minimize noise figure (NF) and maximize gain, while adhering to the LNA's power specifications [17]. This phase includes a thorough analysis of trade-offs among gain, noise figure, and power consumption.

At resonance frequency (operating frequency), voltage gain is represented by Eq. (1):

$$A_V = \frac{V_{out}}{V_s} = \frac{R_{dp}}{2j\omega_o L_s} \tag{1}$$

where R_{dp} is the parallel parasitic resistance of load inductor L_d, ω_o is the resonance frequency, and L_S is the source inductor.

The voltage gain relies on R_{dp}, L_d, and L_S. The real part of Z_{in} is also affected by L_S; therefore, L_s must be selected carefully to avoid excessive gain reduction. The IDCS noise figure is defined by Eq. (2) [18-20].

$$F = 1 + \left(\frac{\omega_o}{\omega_t}\right) \cdot Noise\ ScalingFactor \tag{2}$$

where F represents the noise factor, ω_o denotes the resonance frequency, and $\omega_t = 2\pi f_t$ (where f_t denotes the transistor's cut-off frequency, described as $f_t \cong \frac{g_m}{C_{gs}}$).

$$Noise\ Scaling\ Factor = \gamma\left(\frac{g_{do}}{g_m}\right)\frac{1}{Q_{in}}\left(1 - 2|c|x_d + (4Q_{in}{}^2 + 1)x_d^2\right) \tag{3}$$

where γ represents the excess noise factor, generally about two-thirds in long-channel devices; g_{do} is the channel resistance when $V_{ds} = 0$, δ denotes the gate noise coefficient, typically considered as 2γ; and c indicates the correlation coefficient for the association

between the gate-induced noise current and drain thermal noise current and is approximately 0.395j. The term x_d is defined in Eq (4):

$$x_d = \frac{g_m}{g_{do}} \sqrt{\frac{\delta}{5\gamma}} \tag{4}$$

Q_{in} is the quality factor of the input impedance matching network of IDCS. Because it appears as a series RLC circuit, Q_{in} is expressed as below:

$$Q_{in} = \frac{1}{2R_s \omega_o C_{gs}} \tag{5}$$

Moreover, the key to achieving low noise figure and maximum gain is the careful choice of RF inductors, which impacts noise figure and gain. Important considerations include the inductor's value and quality factor at the operating frequency, along with its self-resonance frequency, which should be remarkably distinct from the operating frequency to avoid resonance from parasitic capacitance. To calculate the optimal device size and biasing voltages for minimum noise figure and maximum gain, Eq. (6), which generally expresses the noise factor, should be discussed [15, 21].

$$F = F_{min} + \frac{R_n}{G_s} |Y_s - Y_{opt}|^2 \tag{6}$$

where F_{min} is the minimum noise factor is given in Eq. (7), R_n denotes noise resistance, G_s represents source conductance, and Y_s and Y_{opt} are source and optimum admittance, respectively.

$$F_{min} = 1 + \frac{2}{\sqrt{5}} \frac{\omega}{\omega_t} \sqrt{\gamma\delta(1 - |c|^2)} \tag{7}$$

To achieve a minimum noise figure, two parts of Eq. (6) must be satisfied. Minimizing noise figures involves first achieving minimal noise in the core transistor through optimal biasing voltages and sizing and then adjusting the input matching circuit so that Y_s is equal to Y_{opt}. Raising the cut-off frequency (f_t) further reduces noise figure in the core transistor.

In the third step, biasing is fine-tuned to optimize power use while balancing its impact on gain, noise figure, and linearity. In an LNA, managing power consumption is crucial for IoT applications because of the distinct operational needs of these devices, such as operating in energy-sensitive, remote environments within the IoT ecosystem. In IoT nodes, LNAs play a critical role by first amplifying weak sensor signals and then processing them further. Consequently, power efficiency is a key factor directly influencing the overall energy budget, longevity of battery-powered IoT devices, and the functionality of these devices, particularly in remote or energy-restricted environments. Although reducing power consumption is vital, achieving and maintaining optimal performance, determined by gain, noise figure, and linearity, is equally critical. This proposed LNA is optimally designed to meet these specific requirements, in addition to allowing efficient power usage for a wide array of IoT applications.

In the final step, which is a crucial phase in LNA designing, matching networks are created. Impedance matching reduces reflections and optimizes noise figure and gain. An inherent trade-off occurs in balancing impedance matching, gain, and noise figure. To minimize noise figure, the input matching network is designed to make Y_s match Y_{opt}, while for maximum gain, it should ensure that input admittance (Y_{in}) matches conjugate source admittance (Y_s^*).

The LNA input can come directly from the antenna or the output of the band-pass filter (BPF) (the duplexer). Because antennas typically have a 50 Ω characteristic impedance, the BPF

should match this 50 Ω impedance for efficient transfer of power from the antenna to the LNA through the BPF. Using the IDCS topology allows for an easy match to the source impedance at the operating frequency without degrading amplifier's noise performance, which is the key advantage of this method.

The input impedance equation for IDCS is given as follows:

$$Z_{in} = S(L_s + L_g) + \frac{1}{SC_{gs}} + \frac{g_m * L_s}{C_{gs}} \qquad (8)$$

where L_s is the source inductor, L_g is the gate inductor, C_{gs} denotes the gate-to-source capacitance, and g_m is the transconductance of the transistor. The first term $S(L_s + L_g)$ represents the inductive reactance from the source and gate inductors. The second term $\frac{1}{SC_{gs}}$ represents the capacitive reactance due to the gate-to-source capacitance.

The third term $\frac{g_m * L_s}{C_{gs}}$ accounts for the impact of the transistor's transconductance and source inductance on the input impedance.

Matching the input impedance to 50 Ω requires setting $Re(Z_{in}) = \frac{g_m * L_s}{C_{gs}}$ to 50 Ω, which depends on the input transistor's g_m, L_S, and C_{gs}. Additionally, the imaginary component of Z_{in}, $I_m(Z_{in}) = S(L_s + L_g) + \frac{1}{SC_{gs}}$, should be zero at the operating frequency, which is attained by balancing $(L_s + L_g)$ with C_{gs} [22].

A trade-off also exists between the design area and input matching circuit. On-chip components save space but often possess a lower quality factor, impacting gain and noise. Off-chip components with a higher quality factor allow more flexibility in matching but require more space.

To achieve input impedance that matches with minimal area usage, the C_{gs} value can be increased by enlarging the transistor, though this also increases the noise figure and power consumption.

To counter this, an external capacitor (C_{ex}) is added between the gate and source, allowing for input impedance matching with low power usage while conserving space [19, 23]. Now, the input impedance is expressed as follows:

$$Z_{in} = S(L_s + L_g) + \frac{1}{S(C_{gs} + C_{ex})} + \frac{g_m * L_s}{(C_{gs} + C_{ex})} \qquad (9)$$

For power transfer and gain to be maximum at the target frequency, the output matching circuit is tuned by selecting an appropriate drain inductor (L_d) to match with the output capacitance (C_L), which includes the parasitic capacitances of the cascode transistor and any following stages (buffer). A chart summarizing the design steps is shown in Fig. 5.

The proposed LNA is designed to operate in IoT-based environments, which impose strict constraints on power consumption, sensitivity, and size. IoT applications often rely on battery-powered devices, making low-power operation a crucial factor. The LNA must achieve ultra-low power consumption while maintaining adequate gain and noise performance to ensure long-term device operation [24]. Additionally, IoT communication protocols, such as Bluetooth Low Energy (BLE), Zigbee, and LoRa, require RF front-end components that can operate efficiently under low-voltage supply conditions. The proposed LNA design incorporates a low-voltage biasing scheme to ensure compatibility with power-constrained IoT nodes [25]. Furthermore, IoT environments involve diverse operating conditions, including variations in temperature and wireless interference. The LNA must be designed to exhibit high linearity and robustness to maintain signal integrity in dense network

deployments [26]. The Inductive Degenerated Cascode topology used in this design ensures stable impedance matching and minimal signal degradation across a wide frequency range [11].
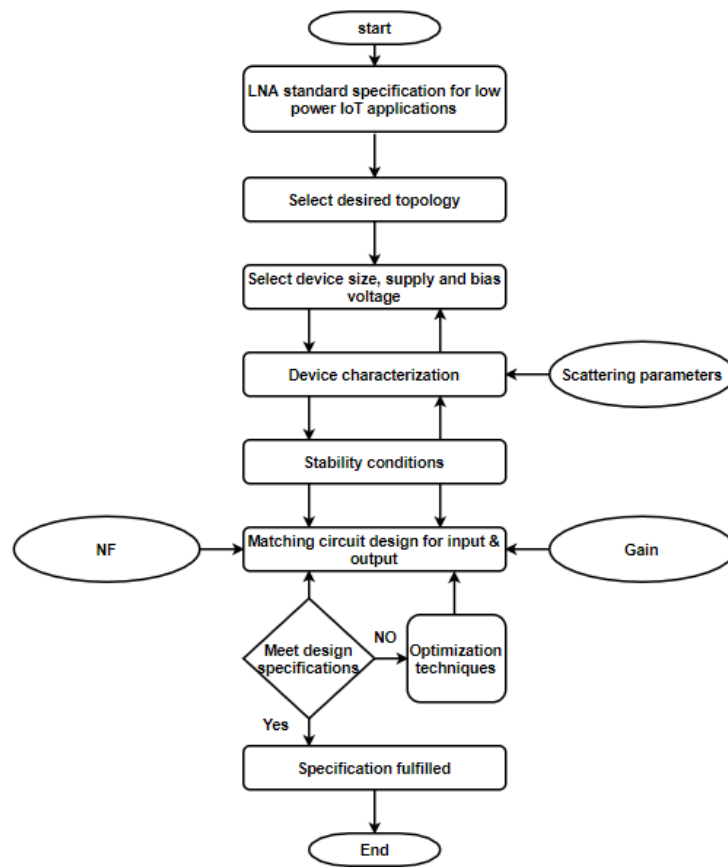

Fig. 5. Proposed LNA design steps.

The proposed LNA design features a source-degenerative cascaded amplifier that utilizes switched transistors, allowing dynamic adjustments to operating conditions through a programmable bias current mirror circuit. This setup enables LNAs to maintain ultra-low power consumption when required, especially in energy-sensitive environments such as TPMS. Fig. 6 depicts the schematic of the designed reconfigurable LNA, including all on-chip components. Inductors L_s and L_g are present in the input stage, along with transistor M_1.
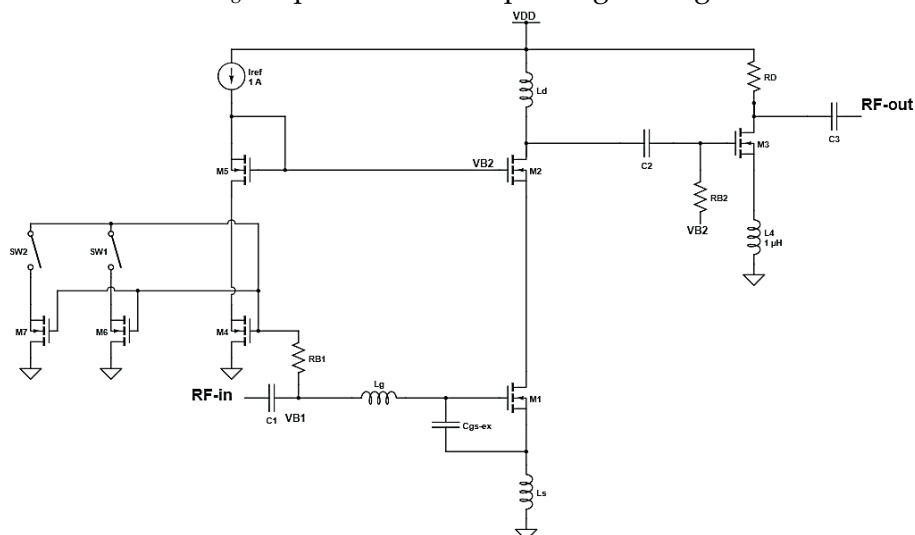

Fig. 6. Fully integrated reconfigurable biasing CMOS LNA for IOT wireless receiver.

The LNA biasing circuit is composed of transistors M_4, M_5, M_6, and M_7. This circuit creates a current mirror to establish bias current with resistor R_B. Noise and power consumption are minimized by setting the widths of these transistors to a small part of the input transistor M_1 [22]. Because the bias current mirror is programmable, switching between modes that prioritize low power consumption or low noise, which is crucial for preserving high sensitivity and reliable signal amplification, is easy.

Furthermore, the output matching network, comprising transistor M2 and drain inductor Ld, delivers high impedance at the operating frequency, thereby allowing optimal gain. For achieving the desired frequency, Ld is adjusted to resonate with the capacitance between the LNA and output buffer, configured as a common source, and the total drain capacitance. The output buffer converts high impedance at M3's gate into low impedance at its drain, which degenerates the source to improve linearity. This comprehensive design, in which n-MOS transistors are used for switching, aids LNA in effectively balancing the trade-offs between power consumption and noise figure, thereby rendering it a versatile and efficient solution for several IoT applications.

6.   THE PROPOSED LNA SIMULATION RESULTS

The proposed LNA was designed using the TSMC CMOS 0.18-µm process design kit (PDK) to ensure realistic modelling of circuit behaviour under actual fabrication conditions and was simulated using the ADS RF circuit simulator at a temperature of 16.85 °C.

In accordance with the simulation results, the LNA could effectively attain low power consumption and high performance in different operational modes. In the low noise-prioritizing Mode 1, 3.2 dB noise figure, 15.62 dB power gain, and 0.87 mW power consumption were attained with LNA. In Mode 2, which provides balanced performance, noise figures reduced to 2.9 dB, gain increased to 17.87 dB, and power consumption optimized at 1.2 mW. Finally, ultra-low power operation is priority in Mode 3, wherein LNA achieved a noise figure of 2.7 dB, a significant gain of 20.52 dB, and a remarkably low power consumption of only 0.1 mW. According to these results, LNA can satisfy application requirements, ensuring that performance is optimal under both low-power and high-performance settings. LNA is thus a perfect option for IoT-based TPMS and related applications. Figs. 7 and 8 below illustrate the simulation results for gain, noise figure, input and output reflection coefficients, stability, linearity, and reverse isolation for the designed LNA in each.

The proposed LNA demonstrates a remarkable level of adaptability and performance across its three operational modes, as highlighted by the simulation results. The design, implemented using the TSMC CMOS 0.18-µm process and simulated under a temperature of 16.85°C, showcases the versatility of the LNA in addressing diverse application requirements, particularly for IoT-based TPMS. Low noise performance was prioritized in Mode 1, the LNA achieved 3.2 dB fand 15.62 dB for noise figure and power gain, respectively while the power consumption maintained low with 0.87 mW. These values indicate that mode is suitable for applications that require minimal signal distortion. In Mode 2, balanced performance was obtained which reflects a design optimized for general-purpose operations. The NF was reduced to 2.9 dB, power gain increased to 17.87 dB, and the power consumption slightly increased to 1.2 mW. Mode 3 focuses on minimizing power consumption, achieving a remarkably low power draw of 0.1 mW. It maintains a noise figure of 2.7 dB and provides an

enhanced gain of 20.52 dB. These results make the mode 3 is most suitable choice for power sensitive applications like Unmanned Aerial Vehicles (UAVs).
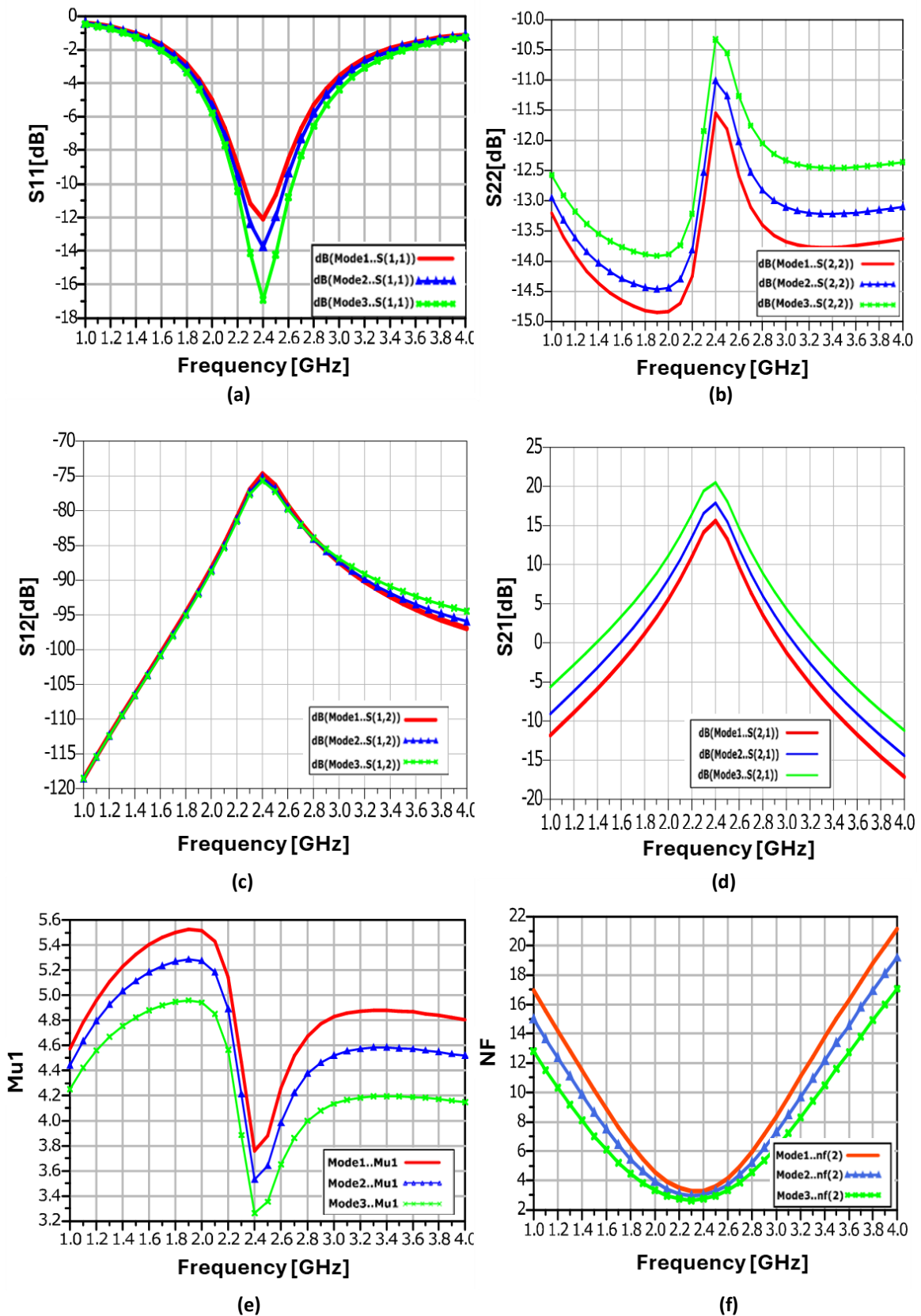

Fig. 7. Simulation results for the reconfigurable LNA: a) input reflection coefficient (S_{11}); b) output reflection coefficient (S_{22}); c) reverse isolation (S_{12}); d) forward gain (S_{21}); e) stability factor; f) noise figure.

The results provide a deeper understanding of the features of the reconfigurable LNA. As indicated, the input (S11) and output (S22) show strong impedance matching in all modes, allowing efficient signal transfer. The revers isolation (S12) stays low, showing strong isolation between input and output, which helps reduce feedback. The forward gain (S21) improves significantly across modes, highlighting the LNA's ability to deliver high performance.

In terms of stability, the simulation results validate that the LNA maintains stable operation across all modes, ensuring reliability in practical applications. The P1-dB performance, as shown in Fig. 8, demonstrates the LNA's linearity under varying input power conditions, with clear differentiation between the modes to suit diverse operational requirements. Additionally, the IIP3 simulation results highlight the LNA's resilience to intermodulation distortion, which is essential for maintaining signal integrity in high-performance communication systems.
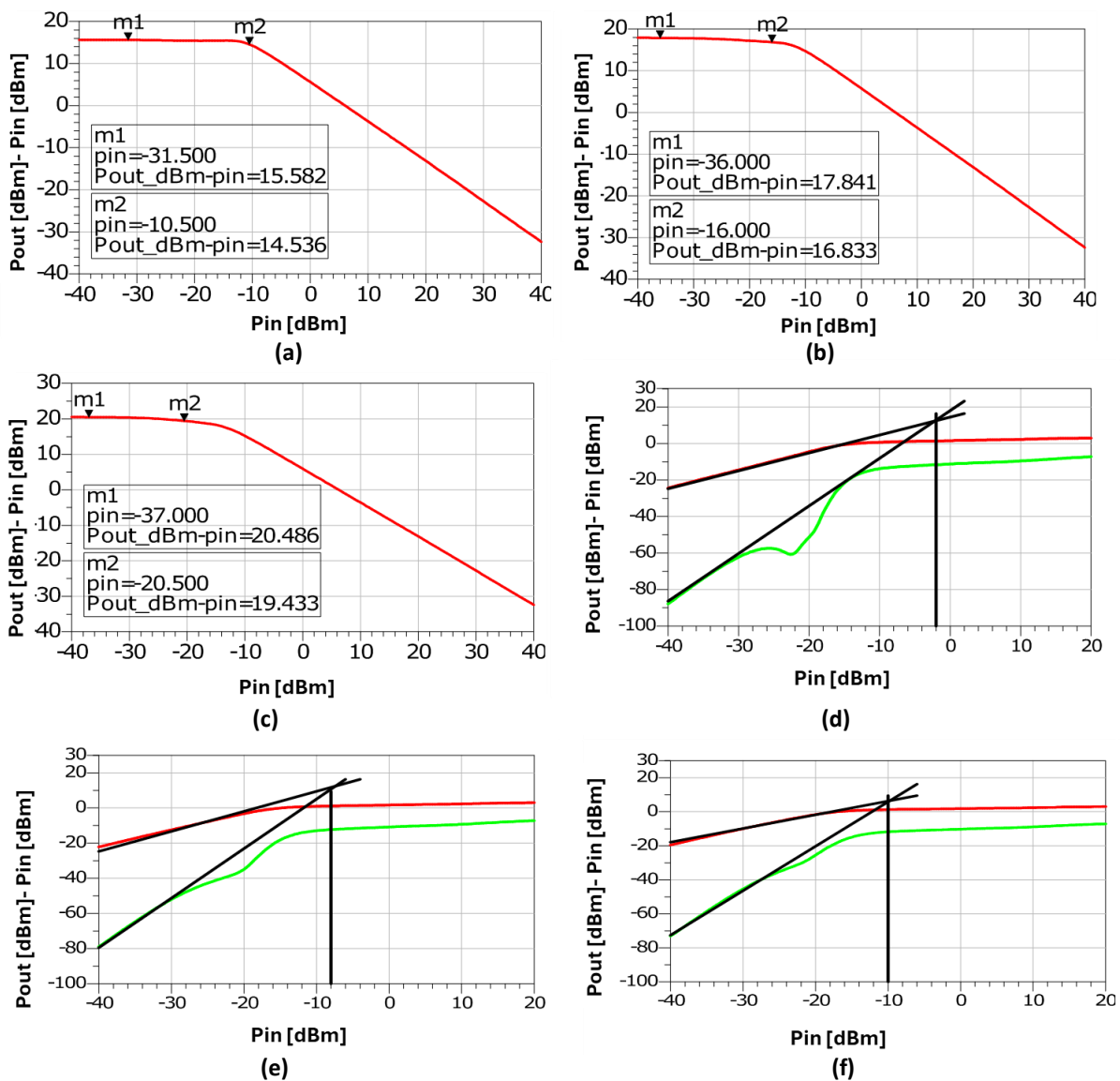
Fig. 8. Simulation results for the reconfigurable LNA: a) P1-dB performance in the first mode; b) P1-dB performance in the second mode; c) P1-dB performance in the third mode; d) IIP3 performance in the first mode; e) IIP3 performance in the second mode; f) IIP3 performance in the third mode.

The simulation results are summarized in Table 1 and compared with other works in Table 2. The comparison shows that the proposed LNA performs better across different

operating modes. In Mode 3, it achieves an impressive noise figure (NF) of 2.7 dB, matching or surpassing many other designs, while delivering a high-power gain of 20.52 dB, which is better than most listed designs A standout feature of the proposed LNA is its exceptional power efficiency consuming only 0.1 mW in Mode 3.

This is much lower than other designs like P1, P3, and P9, which require several milliwatts. The combination of low noise, high gain, and ultra-low power consumption makes the LNA ideal for energy-sensitive applications such as IoT devices like TPMS. These results show that the proposed LNA goes beyond current performance standards, making it a significant step forward for low-power RF circuits.

Table 1. Performance metrics of the proposed LNA across different operating modes.

Pro. LNA	Noise fig. (NF)	Power gain (S21)	1dB Compression point	IIP3	Input reflection coefficient (S11)	Output reflection coefficient (S22)	Reverse isolation coefficient (S12)	Figure of merit (FoM)	Power [mW]
Mode 1 (SW1: off, SW2: on)	3.2 dB	15.62 dB 36.47	-10.5 dB	-2 dBm 0.63 mW	-12 dB	-11.54 dB	-74.74 dB	28.58	0.87
Mode 2 (SW1: on, SW2: off)	2.9 dB	17.87 dB 61.23	-16 dB	-8 dBm 0.158 mW	-13.7 dB	-11 dB	-75.24 dB	10.2	1.2
Mode 3 (SW1: off, SW2: off)	2.7 dB	20.52 dB 112.2	-20.5 dB	-10 dBm 0.1 mW	-16.9 dB	-10.32 dB	-75.68 dB	9.36	1.7

To ensure a fair comparison with state-of-the-art designs that include post-layout results, it is important to acknowledge that post-layout simulations typically exhibit a slight degradation in performance due to added parasitic effects. However, since the proposed LNA is designed using the TSMC 0.18-μm PDK library, the difference between pre-layout and post-layout results is expected to be minimal.

The TSMC 0.18-μm process has well-characterized parasitic models within the PDK, ensuring that simulation results closely match post-layout behavior [27-28].

Additionally, layout-dependent parasitics, such as interconnect capacitances, resistive losses, and mutual coupling effects, can influence the LNA's noise figure (NF) and gain. These parasitics can introduce additional losses, slightly degrading gain and increasing the noise figure due to added resistance and unintended signal coupling [29].

While these effects were not explicitly included in our pre-layout simulations, the well-characterized parasitic models within the TSMC 0.18-μm PDK ensure minimal discrepancy. To further validate the impact of layout parasitics, future work will include post-layout simulations.

Table 2. Comparative performance analysis of the proposed LNA and state-of-the-art designs.

Ref.	Noise fig. (NF)	Power gain (S21)	1dB Comp. point	IIP3	Input reflection coefficient (S11)	Output reflection coefficient (S22)	Reverse isolation coefficient (S12)	Figure of merit (FoM)	Power
Proposed LNA – Mode 1	3.2 dB	15.62 dB 36.47	-10.5 dB	-2 dBm 0.63 mW	-12 dB	-11.54 dB	-74.74 dB	28.58	0.87 mW
Proposed LNA – Mode 2	2.9 dB	17.87 dB 61.23	-16 dB	-8 dBm 0.158 mW	-13.7 dB	-11 dB	-75.24 dB	10.2	1.2 mW
Proposed LNA – Mode 3	2.7 dB	20.52 dB 112.2	-20.5 dB	-10 dBm 0.1 mW	-16.9 dB	-10.32 dB	-75.68 dB	9.36	1.7 mw
[30]	8.2 dB	49.5 dB	<-20 dB	-25.75 dBm	<-10 dB	<-10 dB	-	-	2.16 mW
[31]	2.8 dB	15 dB	−23 dBm	−8.8 dBm	<-10 dB	-	-	39.74 dB	36 μW
[32]	3.6 dB	19.6 dB	-	<−8.5 dBm	<-10 dB	-	-	5.58 dB	3 mW
[33]	3-3.4 dB	13-14.5 dB	-	-2 dBm	<-10 dB	<-25 dB	-	-	15 mW
[34]	3.2 dB	14.7 dB	<−18 dBm	-4.5 dBm	>10 dB	-	-	-	5.1 mW
[35]	2.78-dB	11.46 dB	-	-	<-10 dB	<-10 dB	-	-	2.76 mW
[36]	1.086 dB	9.94 dB	-	8.81 dBm	<-8.5 dB	-	-	11.36	493 μW
[37]	<3.5 dB	13–15.6 dB	<0 dBm	-	<-10 dB	-	<-30 dB	-	21 mW
[38]	1.2 dB	14.55 dB	-16.43 dBm	-22.4 dBm	-14.15 dB	-10.6 dB	-19.4 dB	0.12	9.68 mW
[39]	2.62 dB	18.24 dB	-	-	-15.95 dB	-13.89 dB	-46.05 dB	-	48 mW
[40]	8.7 dB	14.1 dB	-14.6 dBm	-	-14 dB	-	-	-	2 mW
[41]	2.58 dB	16.63 dB	-	-12.53 dBm	-17.41 dB	-	-	2	3.75 mW
[42]	3.14 dB	12.68 dB	-	-	-13.5 dB	-10	-33.85	-	-

7. CONCLUSIONS

An ultra-low power LNA specifically designed for IoT-based TPMS was designed and simulated. In this design, the IDCS topology is picked due to its low power consumption, which is crucial for IoT applications. In addition, with this topology both low noise figure and high gain were achieved. According to the simulation results, the developed LNA exhibited superior performance, featuring 2.7 dB noise figure, 20.52 dB gain, and only 0.1 mW power consumption. Thus, the proposed LNA boosted the performance and energy efficiency of TPMS devices, hence could help augmenting vehicle safety and broadening the field of IoT

applications. A future work may focus on additional optimization of power efficiency and signal fidelity in IoT applications by utilizing different or proposing new topologies that might run on lower power supplies.

REFERENCES

[1] L. Silalahi, M. Alaydrus, A. Muhtar, "Design of tire pressure monitoring system using a pressure sensor base," *SINERGI Journal,* vol. 23, no. 1, p. 70, 2019, doi: 10.22441/sinergi.2019.1.010.

[2] A. Azizan, S. Murad, R. Ismail, M. Yasin, "A review of LNA topologies for wireless applications," 2nd International Conference on Electronic Design, 2014, doi: 10.1109/ICED.2014.7015822.

[3] R. Agrawal, "The review paper on different topologies of LNA," International Conference on Smart Energy and Advancement in Power Technologies, 2022, doi: 10.1007/978-981-19-4975-3_5.

[4] M. Bhuiyan, M. Hossain, M. Rahman, K. Hossain, M. Reaz, R. Begum, K. Minhad, M. Dawi, J. Tan, M. Miraz, "CMOS low noise amplifier design trends towards millimeter-wave IoT sensors," *Ain Shams Engineering Journal,* vol. 15, no. 2, p. 102368, 2024, doi: 10.1016/j.asej.2023.102368.

[5] A. Zuhair, Z. Zakaria, A. Salleh, A. Al-Hadi, "A comparison of low noise amplifiers design and techniques," *ARPN Journal of Engineering and Applied Sciences,* vol. 12, no. 7, pp. 8077–8081, 2017.

[6] *National Highway Traffic Safety Administration*, 2005, http://www.tireindustry.org/pdf/ TPMS_FinalRule_v3.pdf.

[7] S. Govindjee, "Firestone tire failure analysis," *UC Berkeley Civil and Environmental Engineering*, 2001, https://faculty.ce.berkeley.edu/sanjay/REPORT_WEB_Secure.pdf.

[8] M. Brzeska, G. Chakam, "RF modelling and characterization of a tyre pressure monitoring system," 2nd European Conference on Antennas and Propagation, 2007, doi: 10.1049/ic.2007.0879.

[9] H. Song, J. Colburn, H. Hsu, R. Wiese, "Development of reduced order model for modeling performance of tire pressure monitoring system," IEEE Vehicular Technology Conference, 2006, doi: 10.1109/VTCF.2006.608.

[10] N. Savić, M. Junghans, M. Krstić, "Traffic data collection using tire pressure monitoring system," International Conference on Transport Systems Telematics, 2014, doi: 10.1007/978-3-662-45317-9_3.

[11] R. Jaradat, F. Shahroury, H. Shahroury, I. Abuishmais, "Design methodology for narrow-band low noise amplifier using CMOS 0.18 μm technology," *Jordanian Journal of Computers and Information Technology,* vol. 8, no. 1, pp. 98–110, 2022, doi: 10.5455/jjcit.71-1637577305.

[12] S. Patil, R.Kanphade, "Differential input differential output low power high gain LNA for 2.4 GHz applications using TSMC 180nm CMOS RF process," International Conference on Computing Communication Control and Automation, 2015, doi:10.1109/ICCUBEA.2015.181.

[13] K. Xuan, K. Tsang, W. Lee, S. Lee, "0.18 μm CMOS dual-band low noise amplifier for ZigBee development," *Electronics Letters,* vol. 46, no. 1, pp. 85–86, 2010, doi: 10.1049/el.2010.2448.

[14] L. Lu, H. Hsieh, Y. Wang, "A compact 2.4/5.2-GHz CMOS dual-band low-noise amplifier," *IEEE Microwave and Wireless Components Letters,* vol. 15, no. 10, pp. 685–687, 2005, doi: 10.1109/LMWC.2005.856845.

[15] S. Sattar, T. Zulkifli, "A 2.4/5.2-GHz concurrent dual-band CMOS low noise amplifier," *IEEE Access,* vol. 5, pp. 21148–21156, 2017, doi: 10.1109/ACCESS.2017.2756985.

[16] N. Saadallah, S. Alabady, "A Comprehensive study on energy efficient-cluster based routing protocols in the internet of things: hierarchical routing protocol," *Jordan Journal of Electrical Engineering,* vol. 9, no. 3, pp. 369–409, 2023, doi: 10.5455/jjee.204-1670351192.

[17] S. Sharroush, "Analog CMOS design in nanometer regime," *Jordan Journal of Electrical Engineering,* vol. 10, no. 4, pp. 563–593, 2024, doi: 10.5455/jjee.204-1703756483.

[18] D. Shaeffer, T. Lee, "A 1.5-V, 1.5-GHz CMOS low noise amplifier," *IEEE Journal of Solid-State Circuits,* vol. 32, no. 5, pp. 745–759, 1997, doi: 10.1109/4.568846.

[19] P. Andreani, H. Sjöland, "Noise optimization of an inductively degenerated CMOS low noise amplifier," *IEEE Transactions on Circuits and Systems II: Analog and Digital Signal Processing,* vol. 48, no. 9, pp. 835–841, 2001, doi: 10.1109/82.964996.

[20] F. Shahroury, C. Wu, "A 1-V RF-CMOS LNA design utilizing the technique of capacitive feedback matching network," *Integration, the VLSI Journal,* vol. 42, no. 1, pp. 83–88, 2009, doi: 10.1016/j.vlsi.2008.09.007.

[21] A. Antonopoulos, M. Bucher, K. Papathanasiou, N. Mavredakis, N. Makris, R. Sharma, P. Sakalas, M. Schröter, "CMOS small-signal and thermal noise modeling at high frequencies," *IEEE Transactions on Electron Devices,* vol. 60, no. 11, pp. 3726-3733, 2013, doi: 10.1109/TED.2013.2283511.

[22] B. Leung, *VLSI for Wireless Communication*, New York, NY: Springer, 2011.

[23] T. Nguyen, C. Kim, G. Ihm, M. Yang, S. Lee, "CMOS low-noise amplifier design optimization techniques," *IEEE Transactions on Microwave Theory and Techniques,* vol. 52, no. 5, pp. 1433–1442, 2004, doi: 10.1109/TMTT.2004.827014.

[24] Y. Lai, Y. Lai, G. Lee, C. Zheng, P. Huang, M. Lee, Y. Chiang, "Low noise amplifier design for IoT wireless communication systems," IOP Conference Series: Materials Science and Engineering, 2019, doi:10.1088/1757-899X/644/1/012026.

[25] D. Kim, D. Im, "A reconfigurable balun-LNA and Tunable filter with frequency-optimized harmonic rejection for sub-GHz and 2.4 GHz IoT receivers," *IEEE Transactions on Circuits and Systems I: Regular Papers,* vol. 69, no. 8, pp. 3164–3176, 2022, doi: 10.1109/TCSI.2022.3169364.

[26] M. Shafiee, S. Ozev, "An in-field programmable adaptive CMOS LNA for intelligent IoT sensor node applications," *IEEE Transactions on Computer-Aided Design of Integrated Circuits and Systems,* vol. 41, no. 2, pp. 201–210, 2022, doi: 10.1109/TCAD.2021.3077196.

[27] *TSMC 0.18µm Process 1.8-Volt SAGE-X Standard Cell Library Databook*, 2001, https://classes.engineering.wustl.edu/permanant/cse260m/image/Tsmc18_component.pdf

[28] *PDK Reference Manual,* 2004, https://research.ece.cmu.edu/sandbox/referenceManual.pdf

[29] A. Badri, N. Noh, S. Mohd, A. Manaf, A. Marzuki, M. Mustaffa, "Layout effects on high frequency and noise parameters in MOSFETs," *Indonesian Journal of Electrical Engineering and Computer Science,* vol. 6, no. 1, pp. 88–96, 2017, doi: 10.11591/ijeecs.v6.i1.pp88-96.

[30] B. Park, K. Kwon, "2.4-GHz bluetooth low energy receiver employing new quadrature low-noise amplifier for low-power low-voltage IoT applications," *IEEE Transactions on Microwave Theory and Techniques,* vol. 69, no. 3, pp. 1887–1895, 2021, doi: 10.1109/TMTT.2020.3041010.

[31] H. Kooshkaki, P. Mercier, "A 36 µW 2.8–3.4 dB noise figure impedance boosted and noise attenuated LNA for NB-IoT," *IEEE Transactions on Circuits and Systems I: Regular Papers,* vol. 70, no. 1, pp. 101–113, 2023, doi: 10.1109/TCSI.2022.3213504.

[32] S. Tiwari, J. Mukherjee, "An inductorless wideband Gm-boosted balun LNA with nMOS-pMOS configuration and capacitively coupled loads for sub-GHz IoT applications," *IEEE Transactions on Circuits and Systems II: Express Briefs,* vol. 68, no. 10, pp. 3204–3208, 2021, doi: 10.1109/TCSII.2021.3074462.

[33] M. Shafiee, S. Ozev, "An in-field programmable adaptive CMOS LNA for intelligent IoT sensor node applications," *IEEE Transactions on Computer-Aided Design of Integrated Circuits and Systems,* vol. 41, no. 2, pp. 201–210, 2022, doi: 10.1109/TCAD.2021.3077196.

[34] D. Kim, D. Im, "A reconfigurable balun-LNA and tunable filter with frequency-optimized harmonic rejection for sub-GHz and 2.4 GHz IoT receivers," *IEEE Transactions on Circuits and Systems I: Regular Papers,* vol. 69, no. 8, pp. 3164–3176, 2022, doi: 10.1109/TCSI.2022.3169364.

[35] Y. Lai, Y. Lai, G. Lee, C. Zheng, P. Huang, M. Lee, Y. Chiang, "Low noise amplifier design for IoT wireless communication systems," IOP Conference Series: Materials Science and Engineering, 2019, doi:10.1088/1757-899X/644/1/012026.

[36] C. Gladson, A. Narayana, B. Manickam, "An ultra-low-power low-noise amplifier using cross-coupled positive feedback for 5G IoT applications," *SN Applied Sciences,* vol. 1, p. 1470, 2019, doi: 10.1007/s42452-019-1470-8.

[37] S. Blaakmeer, E. Klumperink, D. Leenaerts, B. Nauta, "Wideband balun-LNA with simultaneous output balancing, Noise-Canceling and Distortion-Canceling," *IEEE Journal of Solid-State Circuits*, vol. 43, no. 6, pp. 1341–1350, 2008, doi: 10.1109/jssc.2008.922736.

[38] S. Patil, R. Kanphade, "Differential input differential output low power high gain LNA for 2.4 GHz applications using TSMC 180nm CMOS RF process," International Conference on Computing Communication Control and Automation, 2015, doi: 10.1109/ICCUBEA.2015.181.

[39] P. Bhalse, R. Khatri, "Design of CMOS differential LNA at 2.4 GHz for RF front end receiver," 4th International Conference for Convergence in Technology, 2018, doi: 10.1109/I2CT42659.2018.9057975.

[40] A. Kumar, A. Dutta, B. Sahoo, "A low-power reconfigurable narrowband/wideband LNA for cognitive radio-wireless sensor network," *IEEE Transactions on Very Large Scale Integration (VLSI) Systems,* vol. 28, no. 1, pp. 212–223, 2020, doi: 10.1109/TVLSI.2019.2939708.

[41] Y. Wang, Z. Huang, T. Jin, "A 2.35/2.4/2.45/2.55 GHz low-noise amplifier design using body self-biasing technique for ISM and LTE band application," *IEEE Access,* vol. 7, pp. 183761–183769, 2019, doi: 10.1109/ACCESS.2019.2960177.

[42] N. Shrivastava, R. Khatri, "Design of a 2.4-GHz differential low noise amplifier using 180 nm technology," Proceedings of the IEEE International Conference on Recent Innovations in Signal Processing and Embedded System, 2017, doi: 10.1109/RISE.2017.8378206.